LAWRENCE
LIVERMORE
NATIONAL
LABORATORY

LLNL-JRNL-824979

Tunable Mechanical Matamaterial with Constrained Negative Stiffness for Improved Quasi-Statis and Dynamic Energy Dissipation

C. Morris, L. Bekker, C. Spadaccini, M. Haberman, C. Seepersad

July 27, 2021

Advanced Engineering Materials

Tunable Mechanical Metamaterial with Constrained Negative Stiffness for Improved Quasi-static and Dynamic Energy Dissipation

Clinton Morris, Logan Bekker, Christopher Spadaccini, Michael Haberman, and Carolyn Seepersad*

Dr. C. B. Morris
Palo Alto Research Center, 94304, USA
E-mail: clintonm@parc.com

L. Bekker
Lawrence Livermore National Laboratory, 94550, USA

Dr. C. M. Spadaccini
Lawrence Livermore National Laboratory, 94550, USA

Prof. M. R. Haberman
Mechanical Engineering Department and Applied Research Laboratories, The University of Texas at Austin, 78712, USA

Prof. C. C. Seepersad
Mechanical Engineering Department, The University of Texas at Austin, 78712, USA

Keywords: Mechanical Metamaterial, Materials Design, Negative Stiffness, Microsterolithography

Abstract

This paper presents the computational design, fabrication, and experimental validation of a mechanical metamaterial in which the damping of the material is significantly increased without decreasing the stiffness by embedding a small volume fraction of negative stiffness (NS) inclusions within it. Unlike other systems that dissipate energy primarily through large-amplitude deformation of nonlinear structures, this metamaterial dissipates energy by amplifying linear strains in the viscoelastic host material. By macroscopically tuning the pre-strain of the metamaterial via mechanical loading, the embedded NS inclusions operate about a constrained buckling instability. When further macroscopic vibrational excitation is applied, the inclusions amplify the strains of the surrounding viscoelastic medium. This results in enhanced dissipation of mechanical energy when compared to voided or neat comparison media. Microstereolithography, an emerging high-resolution additive manufacturing

technology, is employed to fabricate the deeply subwavelength inclusions which ensures broadband damping behavior. The mechanically induced broadband energy dissipation and manufacturing approach further differentiate the metamaterial from other approaches that exploit resonances, large deformations, or non-mechanical instabilities. The computational design, fabrication, and experimental evaluation reported is the first dynamic demonstration of such a mechanically tunable NS metamaterial, potentially enabling components with integrated structural and damping capabilities.

1. Introduction

Load bearing components are commonly made from materials with high stiffness to reduce their volumetric profile and weight. Typically, stiff materials do not dissipate mechanical energy efficiently. To address this problem, systems subjected to time-varying loads make use of damping components made of materials with large loss factors, η, to attenuate undesirable broadband vibrations. The introduction of secondary components increases the weight and complexity of the system, which is likely to increase costs and reduce performance, particularly in the aerospace industry.[1] A material with simultaneously high stiffness and loss factor is desirable to reduce the weight or volume of a system. However, this combination of properties does not exist in naturally occurring materials; thus, engineers make a tradeoff between stiffness and damping performance in system design. Composites consisting of metallic or ceramic additives embedded in a polymeric matrix have been investigated to overcome the compromise that must be made between stiffness and loss factor.[2] Unfortunately, the properties of material mixtures are bounded by the behavior of their constituents; thus, traditional composite materials cannot address the need for materials that simultaneously display high stiffness and mechanical loss.[1-4]

Researchers have recently proposed mechanical metamaterials with designed subwavelength structures to generate macroscopic effective properties that exceed the

properties available in naturally occurring materials or traditional composites by increasing loss factors while maintaining stiffness.[5-7] However, most acoustic and mechanical metamaterials derive their exceptional macroscopic properties from microstructural resonances[8-12] such as the metamaterial developed by Fang *et al*. that exhibited a negative effective dynamic modulus as a result of an array of microscale Helmholtz resonators that cause pressure and volumetric strain to be precisely out of phase at the resonance.[8] The reliance on resonance to achieve novel properties restricts the use of metamaterials to narrow bands of operating frequencies and increases susceptibility to internal losses that reduce the macroscopic benefits. In contrast, broadband metamaterials, which typically exploit structural instabilities rather than resonances, can operate within a larger range of dynamic inputs.[3,5,7]

Commonly, structural instabilities are exploited via structured media undergoing reversible buckling events to absorb mechanical energy associated with large deformations[13,14] or high-energy impacts.[15,16] In both cases, the dissipation of energy is associated primarily with the deformation of the buckled structures, which require excitation of sufficiently high amplitude to engender nonlinear deformation to achieve the desired energy absorbing performance. Such large deformation systems, however, may not be feasible in space-constrained environments where large displacements cannot be achieved. This challenge has motivated researchers to explore material architectures that dissipate energy in the presence of small-amplitude disturbances.

Harne *et al.* dissipated energy by embedding mechanically constrained nonlinear structures within a foam.[15,17] The structures are radially-aligned elastomeric elements containing a heavy metallic cylindrical core. The elastomeric elements are initially deformed by insertion into a rigid metallic shell to bring the structure near the buckling limit. External excitations of the foam induced approximately rigid-body motion of the outer rigid shell of the structures which is transferred to the dense core structure via the elastomer that acts as a nonlinear spring element. The combined effect results in energy dissipation for a broad range

of frequencies due to the complex, nonlinear deformation history of the constrained elastomeric elements and inertial effects inside the inclusion. In work analogous to the research presented here, Lakes and coauthors introduced a class of metamaterials that dissipate energy through the inherent mechanical loss mechanisms of a surrounding matrix that constrains an instability that does not rely on inertial effects in the inclusion or matrix.[7] Their original work explored the effect of embedding a small volume fraction of constrained nano-scale ferroelastic inclusions (VO_2) undergoing thermo-mechanical phase transformation within a host metal (Sn). Phase transformation was achieved by thermally loading the composite to produce a strain-induced phase change of the inclusions that resulted in an effective constrained negative stiffness at the inclusion scale and a significant increase the macroscopically observable loss factor.[7] In the presence of a time-varying mechanical deformation, the constrained negative stiffness inclusions amplify the local strain field within the metallic matrix. The small, but measurable, losses of the matrix coupled with the amplified strain resulted in a drastically increased loss factor for the metal composite with minimal changes in stiffness. Unlike the work of Harne *et al.* or other similar nonlinear energy sinks (NES) for Targeted Energy Transfer (TET),[18,19] this class of broadband heterogeneous medium that exploit constrained instabilities is applicable for infinitesimal (i.e. acoustic) disturbances. The macroscopically observable losses are therefore due primarily to the enhanced deformation of the constraining matrix material.[5,7,20].

The current demonstrations of such metamaterials exploiting constrained instabilities rely on inducing the instability via a thermal or magnetic loads.[5,7,9] Such a required load may be prohibitive to apply in many cases. This work presents a mechanical metamaterial that exploits instabilities inherent to the buckling of precisely manufactured curved beam-like elements that increase the macroscopic loss factor when embedded within an appropriate viscoelastic matrix. To induce the instabilities, the metamaterial only requires an initial mechanically prescribed strain, which is common to many engineering applications and

eliminates the need for potentially costly thermal or magnetic preloading schemes. The material properties and improved performance of the metamaterial can therefore be tuned by the initial prescribed strain. Furthermore, the instabilities are manufactured with microstereolithography, an emerging additive manufacturing (AM) technology capable of producing micron-scale features. The demonstration of the use of microstereolithography for metamaterial development motivates future investigation of possible applications afforded by its high-resolution.

2. Design and Fabrication of NS Metamaterial

A representative image of the mechanical structures that serve as negative stiffness inclusions is shown in **Figure 1a**.[10] When the characteristic beam feature of the inclusion is transversely displaced or compressed in the indicated direction the reaction force of the inclusion varies as shown in **Figure 1b**. Once a critical displacement threshold is achieved, the force required to deform the inclusion decreases with increasing displacement, resulting in an incremental negative stiffness. This regime of negative stiffness occurs due to the elastic buckling of the beam and depends on the ratio of the apex height of the beam, h, to the thickness of the beam, t, which may result in monostability or bistability of the inclusion for low or high ratios, respectively.[21] Similarly to the work of Lakes *et al.* in which ferroelastic inclusions are embedded in a metal matrix, these inclusions are embedded within a host matrix to constrain the buckling instability of the beams.[5] Assuming the inclusions are subwavelength and pre-strained into the negative stiffness regime, they act as amplifiers of localized strain within the host material when a macroscopic strain is imposed. The macroscopic strain energy of the viscoelastic host matrix, and thus the loss factor of the heterogeneous medium, are increased without appreciably reducing the overall stiffness.

In previous work, Cortes *et al.* placed similarly defined monostable structures in parallel with a suitable positive stiffness material to induce quasi-zero stiffness resulting in nearly ideal energy absorption that is repeatable and exceeds that of either the positive

stiffness material or the structure alone.[22] To select the precise geometry of the NS structures, nonlinear finite element analysis (FEA) was used to accurately predict the nonlinear stiffness.[22] In an extension of Cortes *et al.* only monostable inclusions are considered in this work, such that they return to their original state once an imposed load is removed.

For modeling purposes, the metamaterial can be posed as a multilevel, hierarchical system, as illustrated in **Figure 1c**.[10] At the smallest scale, referred to here as the micro-scale, the geometry of the inclusion is designed, and its constituent material is selected. Typical inclusions considered here have features on the order of 100 microns with overall bounding dimensions of less than 5 mm. The small inclusion size is necessary to ensure that resulting components contain a sufficient number of inclusions to yield representative storage and loss properties of a mixture. In the intermediate scale, referred to here as the meso-scale, inclusions are embedded within the lossy host material. At this scale, the orientation and volume fraction of the inclusions, material properties of the host matrix, and resultant strain-dependent stiffness of the combined metamaterial are designed to find the macro-scale properties of the metamaterial. Previous work investigated successful modeling strategies for linking the various scales and investigated the impact of parameters such as inclusion geometry and small volume fractions on metamaterial performance.[20] Specifically, FEA-based direct energy homogenization technique was employed to predict the strain-dependent stiffness tensor of the inclusions for specified inclusion geometry and material properties.[23] Previous work by Cortes *et al.* and Debeau *et al.* validated similar nonlinear FEA techniques to accurately predict the performance of NS structures.[16,22] The stiffness tensor obtained from the homogenization model served as an input to an effective medium theory model[24-26] for predicting the loss factor and storage modulus of the metamaterial at a specific frequency for small volume fractions of inclusions.[20] While not employed in this work, the effective medium modelling has been furthered by Konarski *et al.* to predict the frequency-dependent

material properties of NS metamaterials. The work allows for a more precise determination of the effective broadband operating range of such materials including a more accurate model of the low-frequency response including the occurrence of inclusion resonance.[27]

To clarify the aim of developing NS metamaterials, **Figure 1d** provides an Ashby plot illustrating how the performance of conventional materials can be improved in the space spanned by density-normalized storage modulus and loss factor.[28, 29] This figure indicates that heterogeneous effective medium modeling predicts that NS metamaterials can simultaneously exhibit the same or similar stiffness as the host material while drastically improving the loss factor because of the localized strain amplification within the host material that is induced by the inclusions.[5,7] Careful selection of the matrix material and design of the inclusion is necessary to achieve exceptional material properties for the NS metamaterial.

Identification of a suitable inclusion design for desired metamaterial properties is not a trivial task because the design space is mixed continuous-discrete, multilevel, and highly nonlinear. Further, the forward models are computationally expensive and sometimes fail to converge. These features make it difficult to implement optimization-based strategies. Instead, a set-based design methodology that utilizes Bayesian network classifiers was utilized to identify sets of inclusion designs that meet a performance threshold (high loss factor) at the macro-scale.[10, 30] Furthermore, the approach has been augmented to identify sets of inclusion designs that are not only likely to meet the performance threshold but can be reliably manufactured.[31] Incorporation of manufacturing variation to identify the most robust designs is vital, because the process for fabricating the micro-scale inclusions, microstereolithography (**Figure 1e**), induces variation in the geometry of the critical features of the beam as well as the material properties of the inclusion. Critical geometric features and material properties for this work included the apex height and thickness of the beams and the Young's modulus of the material used to fabricate inclusions. These geometric and material property variations were quantified and incorporated into the inclusion design process in previous work.[31, 32] Not

only did the variation inherent to manufacturing inclusions need to be quantified, but a suitable host matrix needed to be identified with the desired positive stiffness. Previous work has indicated that the loss factor is significantly increased when the positive stiffness matrix is approximately equal in magnitude to the negative stiffness of the inclusions. A polyurethane (PU) elastomer (ClearFlex 30 from Smooth-On Inc.,), was selected as such a matrix and used for this work.[5,20,22]

A major difficulty for developing these metamaterials is embedding the inclusions within a host matrix. The specific challenge is simultaneously to ensure sufficient bonding between inclusion and matrix and to prevent the host matrix from penetrating regions of the inclusion that must be evacuated to enable elastic buckling at the micro-scale. The strategy for embedding the inclusions includes the three steps illustrated in **Figure 2a**. In the first step, a mold allowed the PU elastomer to cure while preserving four cubic cavities for the inclusions as well as a critical central clearance hole required for fixturing during dynamic experimentation. In the second step, after the first mold cured, the inclusions were embedded within the cavities and a thin layer of PU was adhered to the top surface of the first mold and the embedded inclusions using a PU-based adhesive. This film formed a seal that prevented the third layer of PU, which was poured over the first two components, from penetrating the cavities that housed the inclusions while maintaining the central clearance hole through the sample. The procedure resulted in an acceptably homogenous host matrix with sufficient bonding to inclusion surfaces. It also ensured that all inclusions were oriented similarly at a 2% volume fraction as assumed in the forward models. The inclusions embedded within the PU matrix are referred to as the *negative stiffness (NS)* sample. Using a similar procedure, a second part was manufactured which contained no inclusions in the cavities and is referred to as the *voided* sample. Then, two final parts were manufactured with identical outer geometry and identical clearance holes to the previous samples but without voids or inclusions; they are referred to as the *control* samples.

3. Experimental Evaluation and Results

After fabricating each of the four samples, their quasi-static behavior was characterized with an MTS Sintech 2/G load frame at an axial compression and release of 1 mm/min over 6 mm in the configuration shown in **Figure 2b**. The results of these tests are shown in the force-displacement plots of **Figure 2c**. While thermosets are notoriously variable in their material properties, there is excellent agreement between the compressive responses of the two control samples. The major difference between the quasi-static responses of the three different types of samples is their hysteretic behavior. **Figure 2d** documents the specific energy absorbed by each of the samples, which was computed as the bounded area of the force-displacement plot shown in Figure 2c. The NS metamaterial clearly absorbs more energy during this quasi-static loading and unloading than the neat materials (Control 1 and Control 2) and the voided material. This result strongly indicates that the NS inclusions embedded within the polyurethane are impacting the quasi-static energy absorption capabilities of the NS polymer. To confirm this conclusion, future work could experimentally determine the nonlinear stiffness tensor of the inclusions. Such a significant effort would require specific machinery such as a micro-indenter and precise fixturing of the micron-scale features of the inclusions to ensure proper boundary conditions are met. However, previous work validating the accuracy of the FEA of this type of NS structure[19,22] and characterizing material properties[30,31] strongly indicates that the properties of NS inclusions are modeled accurately.

Similarly to the initial thermal load provided by Lakes *et al.* or the magnetic field required by Yu *et al.*, an initial mechanical pre-strain was required to tune the material properties the metamaterial of interest;[5, 9] therefore, an experimental apparatus was developed that enabled dynamic testing of the materials at controllable pre-strains. The experimental setup for this purpose is illustrated in **Figure 2e** with an associated schematic shown in **Figure 2f**. The vibration transmissibility of the NS metamaterial, the voided sample,

and the control samples were measured using this system to quantify the damping performance of each sample for varying levels of system pre-strain, $l_{prestrain}$. The experimental setup consisted of five components mounted on a (i) shaker table and located concentrically around a (ii) central bolt that provides the pre-strain. The five concentric components are: (iii) a threaded pre-strain plate which mated with the threads of the central bolt, (iv) the experimental samples (Control 2, Void, or NS), (v) a central mass of aluminum, (vi) a control sample of PU (Control 1), and (vii) a turntable which was mounted directly to the shaker and central bolt. Accelerometers (viii) were placed on the central mass and the turntable to measure the vibration transmissibility of the system, $T(\omega) = u_{cm}\ (\omega)/u_{base}(\omega)$, in which $u_{cm}(\omega)$ and $u_{base}(\omega)$ are the angular frequency-dependent displacements of the central mass and the base, respectively.

By rotating the pre-strain plate, the entire system was compressed to a measurable system pre-strain which would ultimately strain the embedded inclusions, while the turntable minimized shearing of the samples. The experimental samples, central mass, and control sample, as discussed earlier, included sufficiently large central clearance holes such that they could compress and displace axially without contacting the central bolt. The accelerometers measure the vibration transmissibility of the system between the central mass and the turntable through a frequency sweep from 10-700 Hz. In this frequency range, the wavelength in the host material is large compared to the length scale of the inclusions, and the inclusions do not resonate. The samples can therefore be approximated as continuous media with effective stiffness and loss.

Three experiments were performed in which the samples (Control 2, voided, and NS metamaterial) were sequentially mounted in the top half of the apparatus and excited by a frequency sweep at various pre-strains of the system. Control 1 remained in the bottom half of the system throughout all of the experiments. Data from these experiments can be visualized using 3D plots of the magnitude of the transmissibility as a function of the angular frequency

and total system pre-strain, $\epsilon_{prestrain} = \Delta l_{prestrain}/l_{prestrain}$ as shown in **Figure 2g**. The continuous surfaces in Figure 2g are cubic interpolations of transfer function measurements taken at approximately 0.5 mm increments. Higher fidelity measurements (approximately every 0.2 mm of pre-strain) were taken in the region of interest where the amplitude of the transfer function dramatically decreases for the NS metamaterial.

These 3D plots indicate that the system is well approximated using as a single degree of freedom (DOF) damped oscillator. Following the general approach introduced by Norris *et al*.,[33] a forward model given by Equation (1) was developed that relates the frequency-dependent transmissibility, $T(\omega)$, to the material properties, geometry, and pre-strain of the components.

$$T(\omega) = \frac{(RR_k + l_1k_1R_lR_k\csc(l_1k_1)\sin(l_1k_1R_lR_k))}{RR_k\cos(l_1k_1R_lR_k) - \sin(l_1k_1R_lR_k)\,(ml_1P_1(1 + RR_lR_k^2) - \cot(l_1k_1))} \qquad (1)$$

A subscript of 1 indicates a variable is associated with the bottom sample while a subscript of 2 indicates the top sample in Figure 2f. In Equation (1), the complex wave numbers are defined as $k_i = (\rho_i\omega^2/(E_i(1 + j\eta_i))^{1/2}$, in which ρ_i is the density of a sample and E_i and η_i are the storage modulus and loss factor of a sample , respectively. Furthermore, the compressed length of a sample, l_i, can be used to define the length ratio, $R_l = l_1/l_2$ and the other two dimensionless ratios are defined as follows, $R = E_2(1 + j\eta_2)/E_1(1 + j\eta_1)$ and $R_k = k_2/k_1$.

This forward model assumes cylindrical symmetry and axial strains, ignores the effect of the clearance hole, and assumes no shearing tractions at the interface. While the later three assumptions are clearly approximations of the experimental setup, removing any of these assumptions increases the modeling complexity drastically,[34, 35] especially the incorporation of the clearance hole.[36] Finite element modeling is not straightforward due to lack of knowledge of the traction and the viscoelastic response of the polymer. The simplified model is therefore used as a means to provide reasonable estimates of the material properties of the

samples based on the measured response, and therefore to enable comparisons rather than to provide definitive predictions. The derivation of the forward model can be found in the Supporting Information.

At resonance, the real component in the denominator of Equation (1) is equal to zero, resulting in the magnitude of the transfer function being proportional to the inverse of the loss factor of the material.[37] The larger the effective loss factor, the lower and more broadband the transmissibility magnitude at resonance. Leveraging these two facts and extracting the resonance frequency and bandwidth of resonance of the transfer function at each level of initial compression allows the storage modulus and loss factor at resonance to be inferred through inversion. After extracting the frequencies and magnitude of transmissibility at resonance, the natural frequencies were observed to vary from 275-375 Hz and increase with the amount of initial compression. This increase with compression is attributed primarily to the axial shortening of the samples and geometric stiffening, but viscoelasticity relaxation effects may also play a minor role. **Figure 3a** documents the magnitude of the transfer function at resonance for each sample as a function of the initial pre-strain of the experimental sample, $\epsilon_2 = \Delta l_2 / l_2$. The pre-strain of the experimental sample is used rather than the system pre-strain to allow for a better comparison of strain-dependent material properties between the experimental samples. In general, magnitudes at specific pre-strains are consistent across samples, but the magnitude of the NS metamaterial sample is much lower than the other samples at a 0.16 system pre-strain, indicating higher damping. These magnitudes and natural frequencies are then used to infer the storage modulus and loss factor at resonance, which are shown as a function of initial pre-strain of the experimental sample, in **Figure 3b** and **3c**, respectively.

In general, there is excellent agreement in the experimentally determined material properties for all three samples except in the loss factor of the NS metamaterial in the range of strains of the experimental samples from approximately 0.15 to 0.17, corresponding

approximately to the range of 0.11-0.13 system pre-strain. In this pre-strain range, the NS inclusions are constrained to their NS configuration, which leads to increases in cyclic deformation in the neighborhood of the inclusions and substantially increases the effective loss factor when compared to the other samples and the NS samples at different pre-strains. Further, the data also suggests that the activation of the NS inclusions increases the damping capacity of the NS metamaterial without decreasing the storage modulus. It is also important to note that when the NS metamaterial is subjected to strains greater than the NS pre-strain range, the effective loss factor of the metamaterial is once again comparable to the other samples. This behavior is attributed to the curved beam structures in the inclusions being strained past the NS regime and once again displaying positive stiffness, thereby eliminating their benefit. The increased dynamic damping of the metamaterial indicates that the exceptional damping is broadband because it was demonstrated quasi-statically and dynamically across a range of frequencies. Further work should investigate the precise frequency range within which increased damping is achieved, but the preliminary results indicate a broadband damping capability. Konarski *et al.* have been investigating the frequency range within which these NS metamaterials can operate.[27]

To elucidate the behavior of the NS metamaterial, the plots in Figure 2g were modified by converting system strain to experimental sample strain, so cross sections of the experimental sample pre-strain versus properties of interest could be taken for each of the samples and overlaid in Figure 3. These results are shown for two experimental sample pre-strains of 0.06 and 0.16 in **Figure 3d and 3e**, respectively. At the lesser pre-strain, the vibration transmissibility of each sample is in close agreement with respect to both the resonance frequency and magnitude. However, when the metamaterial sample is pre-strained to its NS range, the system is strongly damped, resulting in a significant reduction in the transmissibility magnitude at the resonant frequency. The repeatability of the measurements were investigated by removing the accelerometers and pre-strain plate, re-attaching the

accelerometers, and repeating the experiment. The results are shown in **Figure 3f** which shows excellent agreement between the two separate tests and validates the observation that the pre-strained NS metamaterial is capable of drastically increasing the system loss factor.

4. Concluding Remarks

This initial modeling and experimentation work strongly indicates that a NS metamaterial with enhanced broadband damping and no reduction in storage modulus can be developed by embedding low volume fractions of constrained elastic instabilities within an appropriate matrix and pre-straining them mechanically to their NS regime. The novel NS metamaterial was designed, built, and experimentally demonstrated to be the first mechanically activated NS metamaterial for broadband amplification of losses and minimal changes in stiffness. The mechanical loading contrasts with previous small-amplitude, constrained-instability metamaterials research that required thermal or magnetic loading because mechanical loading is a passive means to induce instability. The successful development of the NS metamaterial required multi-scale design strategies and advanced additive manufacturing, emphasizing the growing focus on integrating advanced computational design strategies with material development.

While the dissipative capabilities of low volume fractions of constrained instabilities are demonstrated in this work, a major barrier to broader application of these metamaterials is the low storage modulus of the elastomeric material used to construct the NS inclusions. Elastomers have low storage moduli and high loss factors relative to metals, which are more commonly used in structural components. It appears that the current inclusion design is insufficient to embed within metals, because the magnitude of negative stiffness is likely be too low to match the positive stiffness of the metals. Future work should therefore investigate NS inclusions that can be embedded within metals to drastically increase the loss factor of structural elements. This motivates future work investigating other inclusion designs or other ferroelastic materials that change phases at or near the ambient temperature.[5,38]

Supporting Information
Supporting Information is available from the Wiley Online Library or from the author.

Acknowledgements

The authors would like to acknowledge support from the National Science Foundation under Grant No. CMMI -1435548 and this work was performed under the auspices of the U.S. Department of Energy by Lawrence Livermore National Laboratory under Contract DE-AC52-07NA27344 (IM# 944586). Michael R. Haberman was partially supported through ONR through MURI grant no. N00014-13-1-0631. We would also like to acknowledge John Cormack for his acoustical expertise, David Debeau for his assistance in experimentation, and Aslan Alamdari, Sumanth Kashyap, and Dr. Jae-Won Choi at the University of Akron for assistance with microstereolithography. The authors thank John Lange for his assistance with the SEM and Jordan Matthews and Tim Klatt for their past assistance in formulating the metamaterials example problem. Any opinions, findings and conclusions or recommendations expressed in this material are those of the authors and do not necessarily reflect the views of the sponsor.

Received: ((will be filled in by the editorial staff))
Revised: ((will be filled in by the editorial staff))
Published online: ((will be filled in by the editorial staff))

References

[1] K. Jayakrishna, V. R. Kar, M. T. Sultan, M. Rajesh, *Materials Selection for Aerospace Components*, Woodhead Publishing, Oxford, UK **2018**.

[2] W. D. Callister, D. G. Rethwisch, *Materials Science and Engineering and Introduction*, Wiley, Hoboken, NJ, USA **2009**.

[3] R. S. Lakes, K. Golden, G. Grimmert, R. James, G. Milton, P. Sen, *Elastic freedom in cellular solids and composite materials*, Springer, NY, USA **1998**.

[4] Onda Corporation, Acoustic tables, http://www.ondacorp.com/tecref_acoustictable.shtml, accessed: February 2016.

[5] Extreme damping in composite materials with a negative stiffness phase, R. S. Lakes, *Physical Review Letters* **2001**, *86(13)*, 2897.

[6] Deformation of extreme viscoelastic metals and composites, Y.C. Wang, M. Ludwigson, R.S. Lakes, *Materials Science and Engineering* **2004**, *370(1-2)*, 41-49.

[7] Extreme damping in composite materials with negative stiffness inclusions, R. S. Lakes, T. Lee, A. Bersie, Y. C. Wang, *Nature* **2001**, *410(6828)*, 565.

[8] Ultrasonic metamaterials with negative modulus, N. Fang, D. Xi, J. Xu, M. Ambati, W. Srituravanich, C. Sun, X. Zhang, *Nature Materials* **2006**, *5(6)*, 452.

[9] Magnetoactive acoustic metamaterials, K. Yu, N. X. Fang, G. Huang, Q. Wang, *Advanced Materials* **2018,** *30(21)*, 1706348.

[10] Hierarchical design of negative stiffness metamaterials using a Bayesian network classifier, J. Matthews, T. Klatt, C. Morris, C. C. Seepersad, M. R. Haberman, D. W. Shahan, *Journal of Mechanical Design* **2016**, *138(4)*, 041404.

[11] Acoustic Metamaterials, M.R. Haberman, M.D. Guild, *Physics Today* **2016**, *69(6)*, 42-48.

[12] Controlling sound with acoustic metamaterials, S.A. Cummer, J. Christensen, A. Alù, *Nature Reviews Material* **2016**, *1(3)*, 16001.

[13] Design, fabrication, and analysis of lattice exhibiting energy absorption via snap-through behavior, C. S. Ha, M. E. Plesha, R. S. Lakes, *Materials and Design* **2018**, *141,* 426-437.

[14] Negative stiffness honeycombs for recoverable shock isolation, D. M. Correa, T. Klatt, S. Cortes, M. R. Haberman, D. Kovar, C. C. Seepersad, *Rapid Prototyping Journal* **2015**, *21(2)*, 193-200.

[15] Resilience to impact by extreme energy absorption in lightweight material inclusions constrained near a critical point, J. Bishop, Q. Dai, Y. Song, R. L. Harne, *Advanced Engineering Materials* **2016**, *18(11)*, 1871-1876.

[16] Impact behavior of negative stiffness honeycomb materials, D. A. Debeau, C. C. Seepersad, M. R. Haberman, *Journal of Materials Research* **2018**, *33(3)*, 290-299.

[17] Trapping and attenuating broadband vibroacoustic energy with hyperdamping metamaterials, R. L. Harne, Y. Song, Q. Dai, *Extreme Mechanics Letter* **2017***, 12*, 41-47.

[18] Inducing passive nonlinear energy sinks in vibrating systems, A. F. Vakakis, *Journal of Vibration and Acoustics* **2001**, *123(3)*, 324-332.

[19] Targeted energy transfer between a model flexible wing and nonlinear energy sink, S. S. Hubbard, D. M. McFarland, L. A. Bergman, A. F. Vakakis, *Journal of Aircraft* **2010**, *47(6)*, 1918-1931.

[20] A nonlinear negative stiffness metamaterial unit cell and small-on-large multiscale material model, T. Klatt, M. R. Haberman, *Journal of Applied Physics* **2013**, *114(3)*, 033503.

[21] A curved-beam bistable mechanism, J. Qiu, J. H. Lang, A. H. Slocum, *Journal of microelectromechanical systems* **2004**, *13(2)*, 137-146.

[22] Design, manufacture, and quai-static testing of metallic negative stiffness structures within a polymer matrix, S. Cortes, J. Allison, C. Morris, M. R. Haberman, C. C. Seepersad, D. Kovar, *Experimental Mechanics* **2017**, *57(8)*, 1183-1191.

[23] Constituitive modeling of piezoelectric polymer composites, G. M. Odegard, *Acta Materialia* **2004**, *52(18)*, 5315-5330.

[24] Micromechanical modeling of particulate composites for damping of acoustic waves, M. R. Haberman, Y. H. Berthelot, M. Cherkaoui, *Journal of Engineering Materials and Technology* **2006**, *128(3)*, 320-329.

[25] R. M. Christensen, *Mechanics of Composite Materials*, Mineola, New York, USA **2012**.

[26] Micromechanics modeling of composite with ductile matrix and shape memory alloy reinforcement, M. Cherkaoui, Q. P. Sun, G. Q. Song, *International Journal of Solids and Structures* **2000**, *37(11)*, 1577-1594.

[27] Frequency-dependent behavior of media containing pre-strained nonlinear inclusions: application to nonlinear acoustic metamaterials, S. G. Konarski, M. R. Haberman, M. F. Hamilton, *The Journal of the Acoustical Society of America* **2018**, *144(5)*, 3022-3035.

[28] Viscoelastic behavior of heterogeneous media, Z. Hashin, *Journal of Applied Mechanics* **1965**, *32(3)*, 630-636.

[29] J. Jarzynski, *Mechanicsms of Sound Attenuation in Materials*, American Chemical Society, USA **1990**.

[30] Bayesian network classifiers for set-based collaborative design, D. W. Shahan, C. C. Seepersad, *Journal of Mechanical Design* **2012**, *134(7)*, 071001.

[31] Design exploration of reliably manufacturable materials and structures with application to negative stiffness metamaterials and microstereolithography, C. Morris, L.

Bekker, M. R. Haberman, C. C. Seepersad, *Journal of Mechanical Design* **2018**, *140(11)*, 111415.

[32] Ultrasonic characterization of the complex young's modulus of polymer parts fabricated with microstereolithography, C. B. Morris, J. M. Cormack, M. R. Haberman, M. F. Hamilton, C. C. Seepersad, *Rapid Prototyping Journal* **2018,** *24(7*), 1193-1202.

[33] D. M. Norris, W.C. Young, *Longitudinal Forced Vibration of Viscoelastic Bars with End Mass,* Cold Regions Research and Engineering Laboratory, Hanover, New Hampshire, USA **1970**.

[34] Discussion: Young's modulus interpreted from compression tests with end friction, S. Watanabe, *Journal of Engineering Mechanics* **1998**, *124(10)*, 1170-1174.

[35] Barreling of solid cylinders under axial compression, J. K. Banerjee, *Journal* of *Engineering Materials and Technology* **1985**, *107(2)*, 138-144.

[36] The development of a new hollow cylinder apparatus for investigating the effects of principal stress rotation in soils, D. W. Hight, A. Gens, M. J. Symes, *Geotechnique* **1983**, *33(4)*, 355-383.

[37] D. Hartog, J. Pieter, *Mechanical Vibrations*, Dover Publications, INC., New York, USA **1985**.

[38] Model free energy, mechanics, and thermodynamics of shape memory alloys, F. Falk, *Acta Metallurgica* **1980**, *28(12)*, 1773-1780.

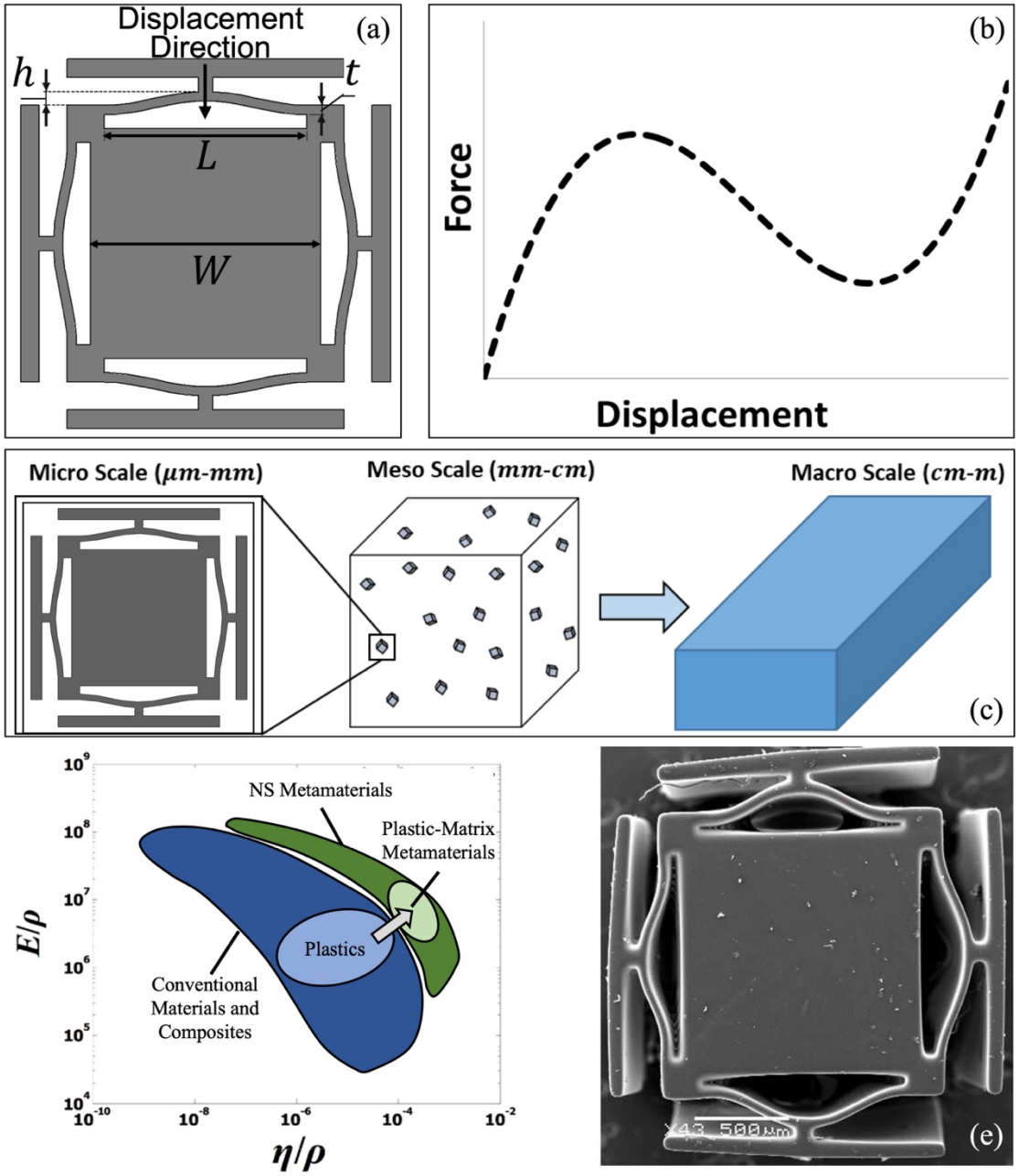

Figure 1. (a) representative image of a negative stiffness inclusion with indicated direction of beam displacement; (b) typical relationship between reaction force and displacement for NS beam when transversely displaced; (c) Schematic illustrating the multilevel and multiscale nature of the design of negative stiffness metamaterial; (d) Ashby plot illustrating the domains of common materials in the space spanned by density-normalized storage modulus and loss factor and the ability for NS metamaterial to improve the loss factor of the host material; (e) Image of a NS inclusion manufactured by microstereolithography captured with a scanning electron microscope.

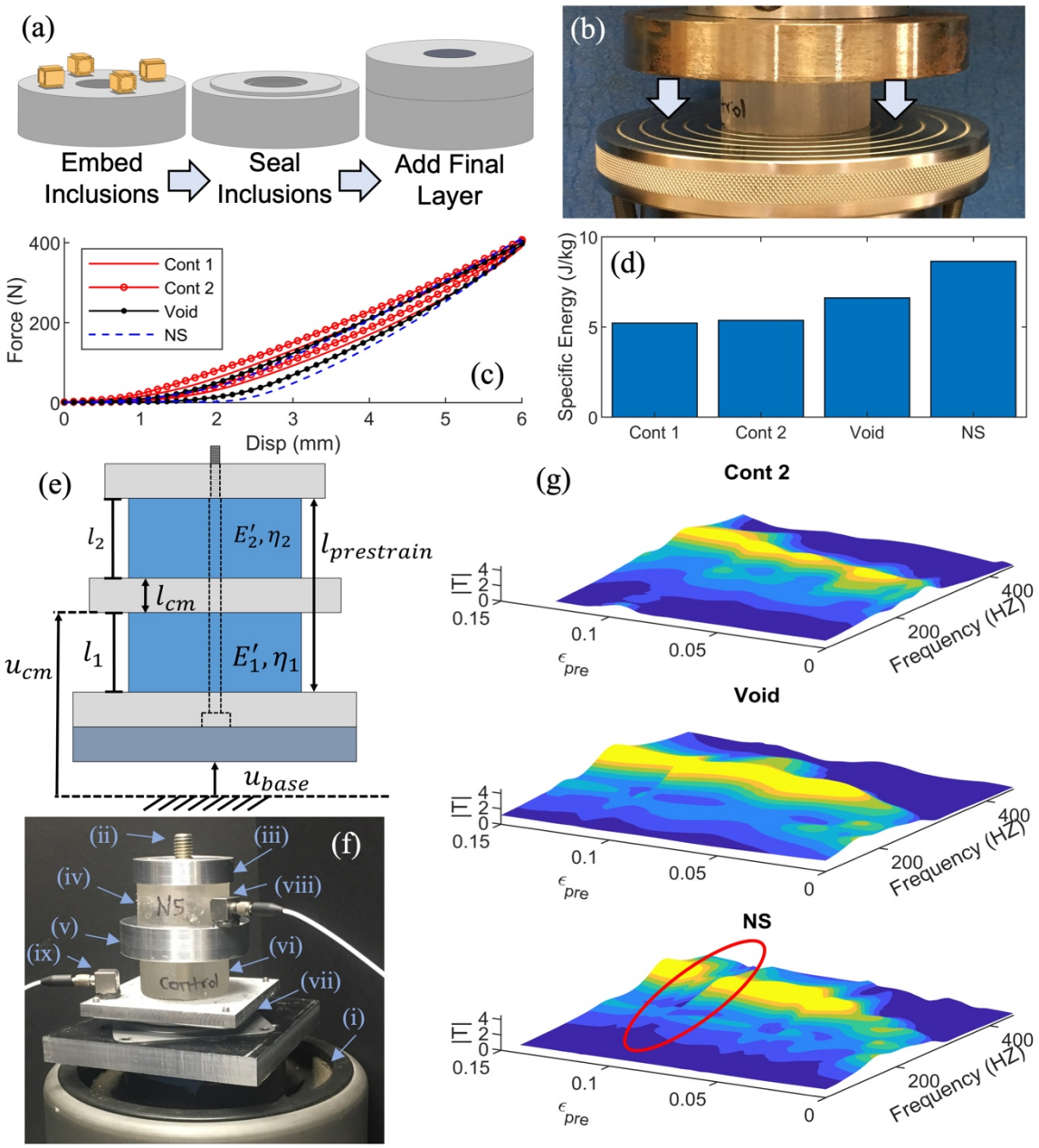

Figure 2. (a) Figure 2: (a) Manufacturing process for the NS metamaterial in which the inclusions are embedded within a molded PU base, sealed with a thin layer of PU, and covered with a final, molded layer of PU; (b) Image of an MTS Sintech 2/G load frame compressing the neat PU material; (c) Quasi-static force-displacement plots for compression testing of Control 1 (red line), Control 2 (red circle) void (black dot), and NS (blue dash) samples; (d) Specific energy absorbed by Control 1, Control 2, Void, and NS samples during quasi-static compression; (e) Schematic of the experimental setup used to determine dynamic material properties; (f) Image of experimental setup for dynamic testing of samples which consisted of five components mounted on a (i) shaker table and located concentrically around a (ii) central bolt. The five concentric components are: (iii) a threaded pre-strain plate, (iv) the experimental samples, (v) a central mass of aluminum, (vi) a control sample of PU, and (vii) a turntable. To measure the transmissibility between the turntable and central mass, (viii and ix) accelerometers were mounted in their respective locations; (g) 3D plots of the magnitude of the transmissibility as a function of the angular frequency and total system pre-strain for each experimental sample. Note the circled region in which the transmissibility drastically decreases within a range of pre-strains.

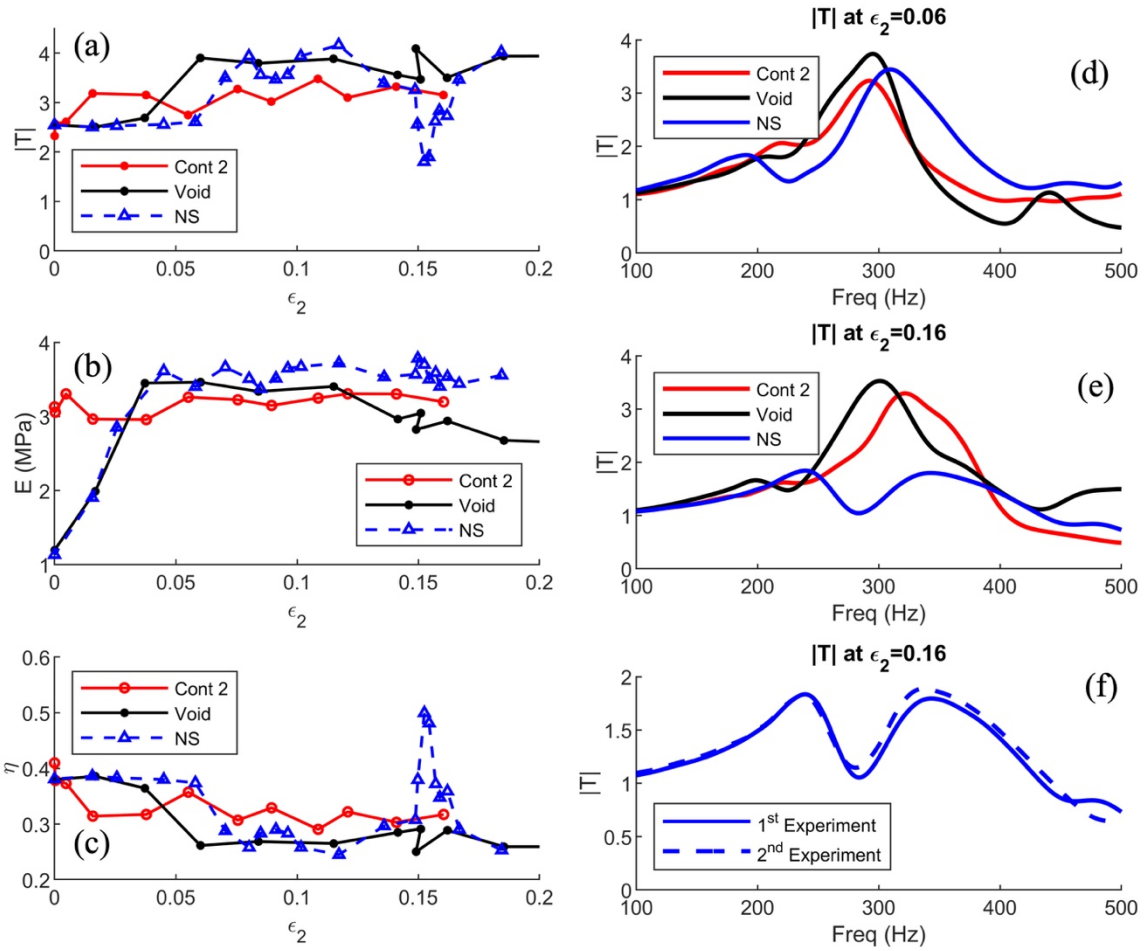

Figure 3. (a) Figure 3: (a) Magnitude of the transfer function at resonance for Control 2 (red circles), Void (black dots), and NS (blue triangle) samples as a function of the experimental sample pre-strain. The decrease and discrepancy in magnitude of the NS sample indicates high damping in the experimental sample pre-strain range of 0.15-0.17; (b) Storage modulus at resonance for Control 2 (red circles), Void (black dots), and NS (blue triangle) samples as a function of the experimental sample pre-strain. Discrepancy at smaller strains is likely due to contact issues during compression ; (c) Loss factor at resonance for Control 2 (red circles), Void (black dots), and NS (blue triangle) samples as a function of the experimental sample pre-strain illustrating increase in loss factor for the NS sample in the sample pre-strain range of 0.15-0.17; (d) Illustration of the agreement in transmissibility of Control 2 (red), Void (black), and NS (blue) samples at $\epsilon_2 = 0.06$; (e) Illustration of the disagreement between the transmissibility of Control 2 (red) and Void (black) samples and the transmissibility of the NS (blue) sample at $\epsilon_2 = 0.16$; (f) Transmissibility of the first NS experiment (solid) and second NS experiment (dashed) at $\epsilon_2 = 0.16$ to illustrate the repeatability of the increased damping. The secondary resonances are attributed to other modes of the experimental setup being excited and were consistent across testing.

ToC

This paper presents the computational design, fabrication, and experimental validation of a mechanical metamaterial in which the mechanical damping of the material is significantly increased by embedding a small volume fraction of negative stiffness (NS) inclusions within it. Unlike other acoustic metamaterials that exploit resonances to enhance damping, the passive mechanical damping reported here occurs across a broad band of frequencies, including quasi-static deformation.

Keywords: *Acoustic Metamaterials*

*L. Bekker, C. M. Spadaccini, M. R. Haberman, C. C. Seepersad, C. B. Morris**

Static and Dynamic Evaluation of a Tunable Acoustic Metamaterial with Constrained Negative Stiffness

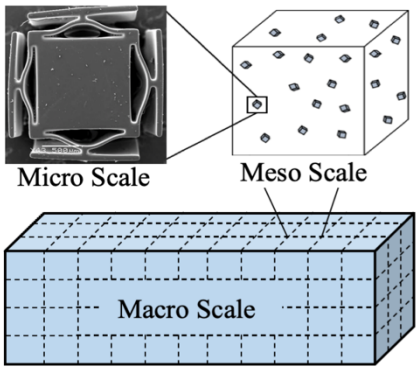

Supporting Information

Derivation of the forward model

*L. Bekker, C. M. Spadaccini, M. R. Haberman, C. C. Seepersad, C. B. Morris**

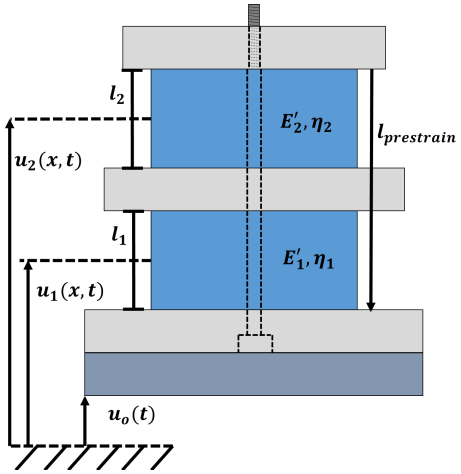

Figure S1. Illustration of the experimental apparatus used to determine the dynamic material properties of the samples.

From **Figure S1** the forced displacement of the base, $u_o(t) = u_b(t)$, the temporally and spatially dependent displacement of the control sample, $u_1(x,t)$, and the temporally and spatially dependent displacement of the experimental sample, $u_2(x,t)$ can be approximated by Equation (S1-S3) in which ω is the input angular frequency, t is time, and x is the spatial variable. Note that $u_1(l_1,t) = u_{cm}(t)$,

$$u_o(t) = U_o e^{j\omega t} \tag{S1}$$

$$u_1(x,t) = U_1(x)e^{j\omega t} + u_o \tag{S2}$$

$$u_2(x,t) = U_2(x)e^{j\omega t} + u_o(t) \tag{S3}$$

For simplicity any off-axes displacements, that is Poisson and geometric effects, are ignored. Therefore this model is certainly inaccurate but can still be used to approximate material properties with error.

Within each sample the constitutive relationship between stress, σ_i, and strain, $\epsilon_i = \partial u_i/\partial x$, shown in Equation (S4) must be obeyed in which E_i and η_i are the storage modulus

and loss factor, respectively. In general the subscript *i* refers to the control sample while the subscript *2* refers to the experimental sample.

$$\sigma_i = E_i(1 + j\eta_i)\frac{\partial u_i}{\partial x} \tag{S4}$$

The equilibrium equations within each sample, given by Equation (S5) must be satisfied in which the density of each sample is ρ_i.

$$\frac{\partial \sigma_i}{\partial x} = \rho_i \frac{\partial^2}{\partial t^2}(u_i + u_o) \tag{S5}$$

By substituting Equation (S5) into Equation (S4) and defining $E_i^* = E_i(1 + j\eta_i)$, Equation (S6) is obtained.

$$E_i^* \frac{\partial^2 u_i}{\partial x^2} = \rho_i \frac{\partial^2}{\partial t^2}(u_i + u_o) \tag{S6}$$

By substituting Equation (S1-S3) into Equation (S6), computing the partial derivative, and eliminating common factors, Equation (S7) is obtained.

$$\frac{\partial^2 U_i(x)}{\partial x^2} + \frac{\rho_i \omega^2}{E_i^*} U_i(x) = -\frac{\rho_i \omega^2}{E_i^*} U_o \tag{S7}$$

By defining, $k_i^2 = \rho_i \omega^2 / E_i^*$, the spatially dependent functions, U_i, are given by Equation (S8).

$$U_i = A_i \cos(k_i x) + B_i \sin(k_i x) - U_0 \tag{S8}$$

To obtain the coefficients, A_i and B_i , of Equation (S8), four boundary conditions are required which are provided by Equation (S9-S12).

$$U_1(0) = 0 \tag{S9}$$

$$U_2(l_1 + l_2) = 0 \tag{S10}$$

$$U_1(l_1) - U_2(l_1) = 0 \tag{S11}$$

$$mk_1^2 l_1(1 + RR_k^2 R_l)(U_1(l_1) + U_o) - \left(\frac{\partial U_1}{\partial x}\bigg|_{x=l_1} + R\frac{\partial U_2}{\partial x}\bigg|_{x=l_1}\right) = 0 \tag{S12}$$

Equation (S9-S11) are simply displacement conditions at the boundaries. Equation (S12) is a force balance on the central mass with mass, M assuming the central mass is a rigid body. The dimensionless ratios, m, R, R_p, and R_l are given by Equation (S13-S16) in which S_i is the surface area of the top surface of the samples.

$$m = \frac{M}{\rho_1 S_1 l_1 + \rho_2 S_2 l_2} \tag{S13}$$

$$R = \frac{E_2^*}{E_1^*} \tag{S14}$$

$$R_k = \frac{k_2}{k_1} \tag{S15}$$

$$R_l = \frac{R_{l_2}}{R_{l_1}} \tag{S16}$$

The four coefficients, A_1, A_2, B_1, and B_2, can then be determined to obtain U_1 and U_2. By determining these functions, the transfer function, $T(\omega)$, between the central mass and the base can be computed and is given by Equation (S17).

$$T(\omega) = \frac{U_1(l_1)}{U_o} = \frac{RR_k + \cot(k_1 l_1)\sin(R_k R_l k_1 l_1) + \sin(R_k R_l k_1 l_1)\tan\left(\frac{k_1 l_1}{2}\right)}{RR_k \cos(R_k R_l k_1 l_1) - \sin(R_k R_l k_1 l_1)\left(mk_1 l_1(1 + RR_l R_k^2) - \cot(R_k R_l k_1 l_1)\right)} \tag{S17}$$